# Experimental Investigation on Bead-on-Plate Welding and Cladding using Pulsed GTAW Process

**Soumak Bose[1] and Santanu Das[2*]**

[1]Department of Mechanical Engineering, Kalyani Government Engineering College, Kalyani - 741235, Nadia, West Bengal, India.

Email ID: [1]soumakbose@gmail.com, [2]sdas.me@gmail.com

* Corresponding author

**DOI: 10.22486/iwj.v54i1.205482**

ORCID: Soumak Bose: https://orcid.org/0000-0002-8835-8722

ORCID: Santanu Das : https://orcid.org/0000-0001-9085-3450



## Abstract

Manufacturing industries intend superior quality production maintaining economy with improved productivity. Components used in engineering applications are desired to have high strength and corrosion resistance for long run reliable performance. Weld cladding is commonly employed on a corrosion prone material with a goal to achieve longer service life of the same. For doing weld cladding, obtaining favourable bead geometry is important, and heat input is expected to play a vital role. In this work, bead-on-plate experiments are first done on low carbon steel substrate using 316 austenitic stainless steel filler employing pulsed GTAW or TIG process. Three-variable Box-Behnken unblocked design of experiment of Response Surface Methodology is resorted to for setting experimental runs. Evaluating appropriate process parameters from this set of experiments, experimental conditions of cladding are set. Corrosion test shows that at 150A welding current, 33Hz welding pulse frequency and 150 mm/min torch travel speed with 0.594 kJ/mm heat input, corrosion rate becomes minimum, and therefore, this parametric combination may be recommended to adopt.

**Keywords:** welding; GTAW-P; Pulsed TIG; cladding; weld bead; corrosion.

## 1.0 Introduction

Reduction of corrosion is a major focus in different industries, etc. to guarantee improved service life of wide category of components, structures, etc. To achieve this, physical or chemical vapour deposition, electroplating, anodizing, cladding, and weld cladding, in particular, etc. may be employed. Except cladding, these coatings are usually thin, and may often break up under an applied load, thereby making the service life low. Weld cladding is applied to create a thick and strong layer to protect base metal from corrosion [1, 2]. In cladding, a thick layer of corrosion resistant material is deposited on a low grade substance [3-6]. Cladding is often harder than the substrate making it abrasion resistant, and then the process is named hardfacing. Cladding is expected not to change the microstructure of the substrate or the clad layer through quite low amount of dilution, while maintaining enough bonding strength [7].

There are different welding techniques, used for cladding, like gas metal arc welding (GMAW), pulsed gas metal arc welding (GMAW-P), gas tungsten arc welding (GTAW), flux-cored arc welding (FCAW), shielded metal arc welding (SMAW), submerged arc welding (SAW), plasma arc welding (PAW), electro slag welding (ESW), laser welding, powder welding by laser, etc. Providing proper heat input, desired mechanical properties of a cladding can be achieved [1, 6-11].

High quality weld joint is obtained by Gas tungsten arc welding (GTAW), or tungsten insert gas (TIG) welding process. However, low penetration of this welding process restricts it for its large application. On the other hand, GTAW cladding giving good aesthetics and quality, can well be used as cladding requires shallow penetration with good bond strength. Again, pulsed GTAW (GTAW-P) or pulsed TIG welding was also tried to improve productivity of GTAW process and also for cladding [1, 7-11]. In practice, there are numerous types of cladding materials available like nickel, copper, cupronickel, stainless steel, aluminium, copper-silver alloy, etc. Among them, stainless steels are well accepted weld cladding material due to their high chromium content. Chromium forms a protective oxide of it on the surface of an iron-chromium alloy to resist corrosion; it makes a stainless steel stainless [9-15]. There are several categories of stainless steel based on crystal structure such as ferritic stainless steel (BCC structure), martensitic stainless steel, austenitic stainless steel (FCC structure), etc.

Beside these, in some cases, duplex stainless steel which is a mixture of 50% Ferrite & 50% austenitic stainless steels were also tried [16].

A number of works was reported on TIG cladding of cobalt-based alloys [3], copper alloys [4], different alloying elements [5], stellite [6], austenitic stainless steel [13], iron-titanium carbide [17], etc. Observation of austenitic stainless steel bead geometry and influence of heat input on weld bead were also investigated [18] on low carbon steel in a work. Pulsed TIG welding for cladding low alloy steel base plate with 309 stainless steel was also reported [1] in a work. In the same report, GTAW-P weld cladding was also compared with plasma arc cladding. Wear characteristics of Fe-Cr-C and Fe-Cr-Nb-C TIG clad layers on carbon steel along with their microstructure were investigated [19] by a group of researchers, while investigation on slow cooling procedure for TIG clad components with stainless steel hot filler wire was done [20] by another research team with some success.

In this work, bead-on-plate experiments are done first on low carbon steel substrate using 316 austenitic stainless steel filler wire by pulsed GTAW (GTAW-P) process using argon gas shield. After getting the appropriate range of process parameters from this experiment, cladding experiments are done. Pitting corrosion test is carried out on clad specimens and the condition corresponding to minimum corrosion is tried to find out in the experimental work done.

## 2.0 Experimental Detail

Popularly used low carbon structural steel plates of the size of 60 mm × 75 mm × 25 mm each are utilized as the substrate material in this investigation. A thickness of 25 mm is made use of to avoid distortion. Chemical composition of this low carbon steel plate is shown in **Table 1**. It has 0.313% of carbon with 0.62% manganese and 0.161% silicon. Rest elements are trace and tramp elements.

Austenitic stainless steel (316) wire (1.2 mm diameter) is used as the filler wire with 15.046% chromium, 9.937% nickel, 2.091% molybdenum and 1.102% manganese. There is also 0.342% copper and 0.182% silicon along with only 0.076% carbon. Chemical constituents of this electrode material are given in **Table 2**.

Table 1 : Composition of the base material

| %C | %Si | %Mn | %P | %S | %Cr | %Mo | %Ni | %Al | %Co |
|---|---|---|---|---|---|---|---|---|---|
| 0.313 | 0.161 | 0.62 | 0.08 | 0.041 | 0.029 | 0.016 | 0.03 | 0.006 | 0.01 |
| %Cu | %Nb | %V | %W | %Sn | %Ce | %B | %N | %Mg | %Fe |
| 0.081 | 0.014 | 0.002 | 0.007 | 0.012 | 0.007 | 0.001 | 0.012 | 0.009 | 98.549 |

Table 2 : Composition of the austenitic stainless steel (316)

| %C | %Si | %Mn | %P | %S | %Cr | %Mo | %Ni | %Al | %Cu |
|---|---|---|---|---|---|---|---|---|---|
| 0.076 | 0.182 | 1.102 | 0.029 | 0.008 | 15.046 | 2.091 | 9.937 | 0.011 | 0.342 |
| %Nb | %V | %Co | %Ti | %W | %Sn | %Ce | %B | %Fe | |
| 0.002 | 0.048 | 0.074 | 0.032 | 0.026 | 0.010 | 0.010 | 0.001 | 70.973 | |

The experimental work is performed on Kemppi, Finland made Master TIG MLS 3003ACDC model of GTAW machine having the facility of pulsing. A cold wire feeder unit having model number CWF 04 is also integrated with the GTAW machine. A motor driven vehicle is used to mount the welding gun, which is capable for speed variation and is driven along a straight guide rail. Welding gun angle is kept constant at an angle of $85^{o}$ to the work table in a vertical plane with the help of a fixture. The experimental set up showing GTAW welding gun with motor driven vehicle is depicted in **Fig. 1**. 99.99% commercially pure tungsten electrode with a diameter of 2.4 mm is fitted inside a standard ceramic nozzle for acting as the non-consumable arc welding electrode. Commercially pure 100% argon is used as the gas shield at a flow rate of 15 lit/min. Process parameters chosen for these experiments and heat input provided are shown in **Table 3**. Welding current (I), torch travel speed (S) and welding pulse frequency are varied at their three levels. Heat input (calculated using equation (1)) is varied from 0.498 kJ/mm to 1.033 kJ/mm.

$$Q = \frac{(V \times 1 \times 60)}{(1000 \times S)} \times \eta \quad (1)$$

Where,
Q = Heat Input (kJ/mm)
V = Voltage (V)
I = Current (A)
S = Torch Travel Speed (mm/min)
η = Efficiency (For GTAW, it taken as 75%)

For measuring bead geometry (width of weld bead, depth of penetration and height of reinforcement), polished and mirror finished samples are observed under the Gippon, Japan made advanced stereo microscope and bead dimensions are noted.

For bead-on-plate test by GTAW-P, the test pieces are made free from rust and cleaned. Then weld beads are generated on these plates by using austenitic stainless steel (316) filler wire with selected process parameters like welding current, welding pulse frequency and torch travel speed. Welding current is varied from 110A to 150A while torch travel speed is varied from 90mm/min to 150 mm/min. Pulsing frequency is varied from 6Hz to 60Hz. The range of process parameters have been chosen based on some prior trial experiments using the same base plate-filler combination under similar welding conditions. Fifteen sets of experimental runs are done to complete this experiment. Two sets of replicated experiments have been done. Parameters for fifteen experimental runs are obtained from three-variable Box–Behnken unblocked design of experiments of Response Surface Methodology (RSM).

Table 3 : Parameters of bead-on-plate experiment by GTAW-P

| Sample No. | Welding Current (A) | Frequency (Hz) | Torch Travel Speed (S) (mm/min) | Heat Input (kJ/mm) |
|---|---|---|---|---|
| 1 | 150 | 33 | 90 | 0.728 |
| 2 | 130 | 60 | 90 | 0.676 |
| 3 | 130 | 6 | 150 | 0.581 |
| 4 | 110 | 60 | 120 | 0.573 |
| 5 | 150 | 60 | 120 | 0.63 |
| 6 | 130 | 33 | 120 | 0.6 |
| 7 | 150 | 33 | 150 | 0.594 |
| 8 | 110 | 6 | 120 | 0.586 |
| 9 | 110 | 33 | 90 | 0.732 |
| 10 | 150 | 6 | 120 | 0.793 |
| 11 | 130 | 60 | 150 | 0.655 |
| 12 | 130 | 33 | 120 | 0.629 |
| 13 | 110 | 33 | 150 | 0.498 |
| 14 | 130 | 6 | 90 | 1.033 |
| 15 | 130 | 33 | 120 | 0.609 |

For cladding, the base plate is first cleaned, and an overlap of 50% of the successive beads is considered. This is done by placing the filler wire around the edge of the preceding bead with the help of a motor driven vehicle, and thus, makes the desired overlapped weld bead for cladding. Weld bead geometry such as depth of penetration (DOP), height of reinforcement (HOR) and weld bead width (WBW) are measured on polished samples under the advanced stereo microscope. Polishing of crosswise cut samples are carried out first on a belt grinder-cum-polisher and disc grinder-cum-polisher with different grades of emery papers. Then disc grinder-cum-polisher is utilized for buffing operation using alumina paste and velvet cloth to make the samples scratch free and mirror-finished.

For pitting corrosion test, test specimens of the clad zone are cut from the workpiece. Exposed areas of test specimens are made of a size of (10×10) $mm^2$ by the help of a grinding machine and a belt grinder. After polishing, specimens are weighed by Wensar, India made digital weighing machine with a maximum weight capacity of 200 gm with a resolution of 1mg. Then, the test specimens are coated by a teflon tape, leaving only the clad area exposed. Each sample is immersed for 24 hours within a corrosive liquid which is a mixture of 30gm ferric chloride, 27 ml HCl and 73 ml distilled water.


Fig. 1 : GTAW welding gun mounted on motor driven vehicle

After removing from the corrosive medium, test specimens are cleaned with running water and then are weighed again after drying. The loss of weight is determined by the difference of initial and final weight of the test sample. Corrosion rate is calculated through equation (2). Counting of number of pits is done using Gippon, Japan made advanced stereo microscope. After cutting and final polishing, work samples are placed on stereo microscope. Making many square blocks of 1 cm x 1 cm upon enlarged image of corroded surface of work samples digitally, and by dividing each block in 16 equal parts, number of pits of all parts is counted, and then total number of pits in

one block is summed up. After calculating number of pits in all blocks, average of all these is made to get number of pits/$cm^2$ over the entire corroded area.

$$\text{Rate of Corrosion} = \frac{W}{A \times T} \quad (2)$$

Where,

W =Loss of weight (gm)

A = Uncovered area ($m^2$)

T = Exposed time (hr)

## 3.0 Results and Discussion

Bead-on-plate experiment and pulsed TIG cladding with 316 austenitic stainless steel filler wire on low carbon steel base plates are performed in this experimental investigation. GTAW-P is expected to yield higher productivity than GTAW process. Bead-on-plate experiments are carried out following three-variable Box–Behnken unblocked design of experiment method of RSM as discussed earlier, and the results observed are discussed in the following sections. From the optimal conditions derived from the bead-on-plate experiments, process variables for cladding experiments are selected.

### 3.1 Bead-on-Plate Experiment

#### 3.1.1 Results of Visual Inspection

**Table 4** shows the visual inspection results of bead-on-plate experiments by GTAW-P. Except three experimental runs corresponding to sample numbers 2, 4 and 10, no spatter is obtained in this experiment. Moderate or few numbers of blow holes are observed in some cases of sample numbers 1-4, 7, 9 and 12. One weld bead of sample number 4 is found to be discontinuous, and this condition will not be considered for further tests. All other conditions showed uniform, acceptable welding. Observed weld bead geometry parameters, such as depth of penetration (DOP), weld bead width (WBW) and height of reinforcement (HOR), are shown in **Table 5**.

#### 3.1.2 Finding out the Effect of Process Parameters on Bead Geometry in Bead-on-Plate Experiment

Multiple regression equations given in equation (3-5) are evaluated following Response Surface Methodology (RSM) using MINITAB 17 software from the data obtained from experiment **Table 5**. The relation of depth of penetration (DOP), height of reinforcement (HOR) and weld bead width (WBW) with welding voltage (V), welding frequency (F) and torch travel speed (S) are given in equation (3), (4) and (5) respectively.

Table 4 : Observations from visual inspection on bead-on-plate made

| Sample No. | Frequency (F) (Hz) | Welding Current (I) (A) | Torch Travel Speed (S) (mm/min) | Heat Input (kJ/mm) | Blow Holes | Spatter | Continuity in Deposition |
|---|---|---|---|---|---|---|---|
| 1 | 33 | 150 | 90 | 0.728 | Few | Nil | Continuous |
| 2 | 60 | 130 | 90 | 0.676 | Few | Medium | Continuous |
| 3 | 6 | 130 | 150 | 0.581 | Few | Nil | Continuous |
| 4 | 60 | 110 | 120 | 0.573 | Moderate | Few | Discontinuous |
| 5 | 60 | 150 | 120 | 0.63 | Nil | Nil | Continuous |
| 6 | 33 | 130 | 120 | 0.6 | Nil | Nil | Continuous |
| 7 | 33 | 150 | 150 | 0.594 | Few | Nil | Continuous |
| 8 | 6 | 110 | 120 | 0.586 | Nil | Nil | Continuous |
| 9 | 33 | 110 | 90 | 0.732 | Few | Nil | Continuous |
| 10 | 6 | 150 | 120 | 0.793 | Nil | Few | Continuous |
| 11 | 60 | 130 | 150 | 0.655 | Nil | Nil | Continuous |
| 12 | 33 | 130 | 120 | 0.629 | Few | Nil | Continuous |
| 13 | 33 | 110 | 150 | 0.498 | Nil | Nil | Continuous |
| 14 | 6 | 130 | 90 | 1.033 | Nil | Nil | Continuous |
| 15 | 33 | 130 | 120 | 0.609 | Nil | Nil | Continuous |

Table 5 : Observed results of bead-on-plate experiments by GTAW-P

| Sample No. | Welding Current, I (A) | Frequency (F) (Hz) | Travel Speed (S) (mm/min) | Weld Voltage V (V) | Heat Input (kJ/mm) | Average depth of Penetration, DOP (mm) | Average Height of Reinforcement HOR (mm) | Average Weld Bead Width WBW (mm) |
|---|---|---|---|---|---|---|---|---|
| 1 | 150 | 33 | 90 | 9.7 | 0.728 | 2.54 | 2.46 | 9.99 |
| 2 | 130 | 60 | 90 | 10.4 | 0.676 | 2.36 | 2.66 | 8.93 |
| 3 | 130 | 6 | 150 | 14.9 | 0.581 | 1.54 | 2.51 | 5.84 |
| 4 | 110 | 60 | 120 | 13.9 | 0.573 | 1.02 | 2.85 | 4.72 |
| 5 | 150 | 60 | 120 | 11.6 | 0.63 | 1.07 | 2.36 | 7.59 |
| 6 | 130 | 33 | 120 | 12.3 | 0.6 | 0.96 | 2.44 | 6.06 |
| 7 | 150 | 33 | 150 | 13.2 | 0.594 | 1.16 | 1.6 | 7.53 |
| 8 | 110 | 6 | 120 | 14.2 | 0.586 | 1.09 | 2.43 | 4.27 |
| 9 | 110 | 33 | 90 | 13.3 | 0.732 | 1.57 | 2.28 | 7.49 |
| 10 | 150 | 6 | 120 | 14.1 | 0.793 | 1.63 | 2.22 | 5.31 |
| 11 | 130 | 60 | 150 | 16.8 | 0.655 | 0.95 | 2.43 | 6.42 |
| 12 | 130 | 33 | 120 | 12.9 | 0.629 | 1.4 | 2.47 | 4.09 |
| 13 | 110 | 33 | 150 | 15.1 | 0.498 | 0.94 | 2.6 | 5.76 |
| 14 | 130 | 6 | 90 | 15.9 | 1.033 | 2.45 | 2.26 | 11.05 |
| 15 | 130 | 33 | 120 | 12.5 | 0.609 | 0.92 | 2.44 | 5.21 |

$$DOP = 16.5 - 0.078\,I - 0.0288\,F - 0.1562\,S + 0.000359\,I*I + 0.000290\,F*F + 0.000418\,S*S - 0.000500\,I*F + 0.000133\,I*S + 0.000552\,F*S \quad (3)$$

$$HOR = 0.99 + 0.0791\,I - 0.0136\,F - 0.0601\,S - 0.000346\,I*I + 0.000177\,F*F + 0.000052\,S*S - 0.000181\,I*F + 0.000242\,I*S + 0.000194\,F*S \quad (4)$$

$$WBW = 26.8 + 0.032\,I - 0.1408\,F - 0.338\,S - 0.000184\,I*I + 0.001082\,F*F + 0.000690\,S*S - 0.001037\,I*F + 0.000663\,I*S + 0.001432\,F*S \quad (5)$$

Where,

I = Welding Current

F = Welding Frequency

S = Torch Travel Speed

Values of $R^2$ of equation (3), equation (4) and equation (5) are 95.78%, 97.39% and 94.39% respectively. These values indicate good relationships signifying the acceptability of these equations.

The contour plot and surface plot of depth of penetration (DOP), height of reinforcement (HOR) and weld bead width (WBW) are shown as the function of welding voltage, welding frequency and torch travel speed as shown in **Fig.2** through **Fig.19**. The contour plot and surface plot of depth of penetration (DOP) with the variation of welding voltage and welding frequency, while torch travel speed is kept constant at the lower value of 90 mm/min, middle value of 120 mm/min and higher value of 150 mm/min are shown in **Fig.2** through **Fig.7** respectively.

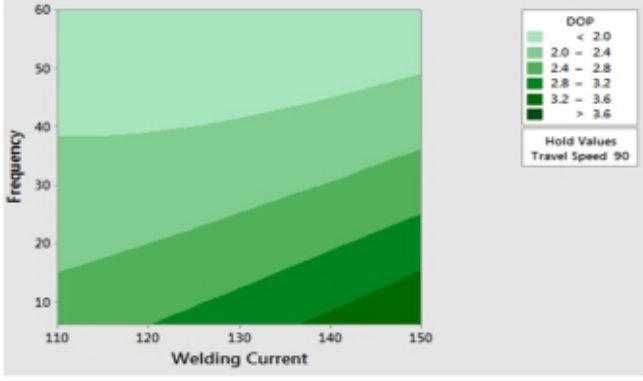


Fig.2 : Contour plot of depth of penetration with welding current and welding frequency at a stable travel speed of 90 mm/min

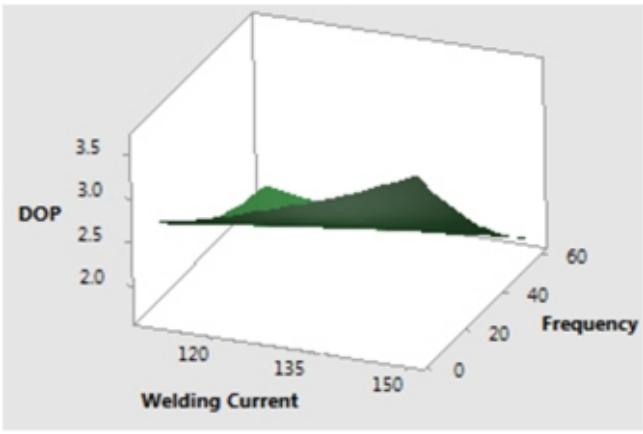


Fig.3 : Surface plot depth of penetration with welding current and welding frequency at a stable travel speed of 90 mm/min

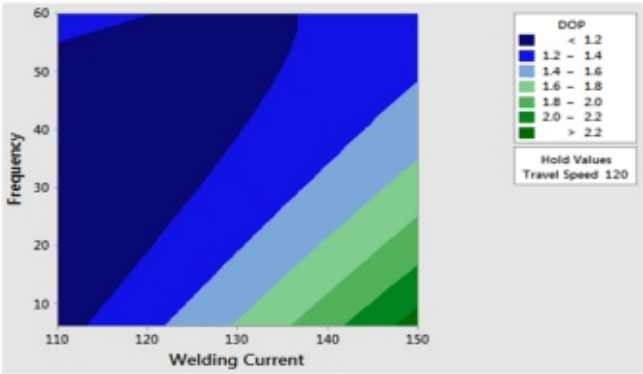


Fig. 4 : Contour plot of depth of penetration with welding current and welding frequency at a stable torch travel speed of 120 mm/min

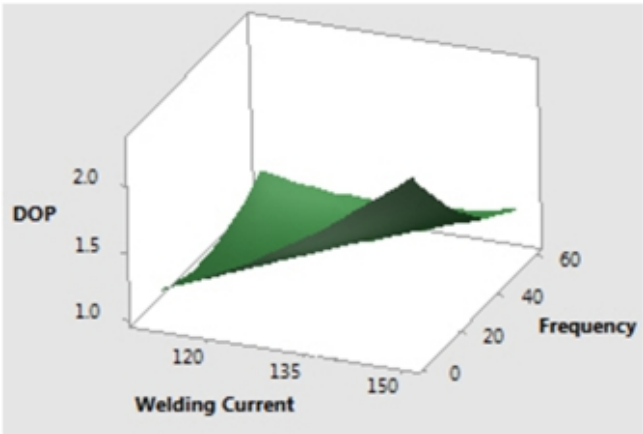


Fig.5 : Surface plot of depth of penetration with welding current and welding frequency at a stable travel speed of 120 mm/min

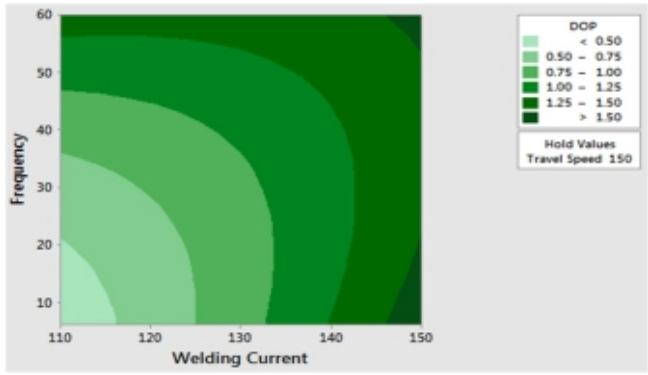


Fig. 6 : Contour plot of depth of penetration with welding current and welding frequency at a stable travel speed of 150 mm/min

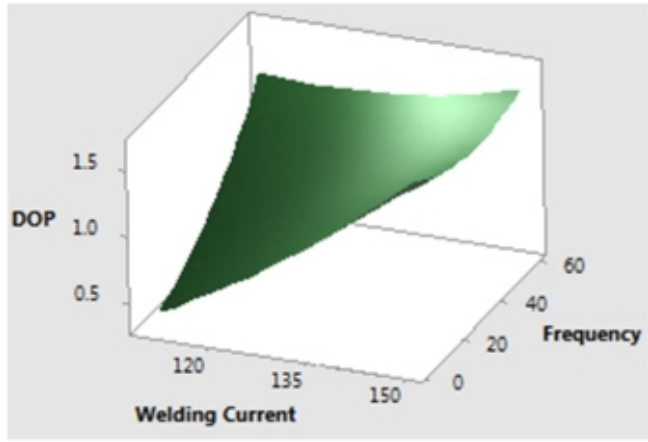


Fig. 7 : Surface plot of depth of penetration with welding current and welding frequency at a stable travel speed of 150 mm/min

In case of constant travel speed of 90 mm/min and 120 mm/min, it can be observed that the highest values of depth of penetration of austenitic steel are in the lower right portion of the plot, which indicates to high values of welding current and low values of welding frequency. The lowest values of depth of penetration for constant torch travel speed of 90 mm/min and 120 mm/min are in the upper left portion of the plot, which indicates low values of welding current and high values of welding frequency. Low current at a constant torch travel speed results in low heat input to the system thereby causing a small volume of molten weld pool and hence, the low depth of penetration. Increase in current gives more heat input, more volume of molten material during welding and high penetration.

In case of constant torch travel speed of 150 mm/min, lowest values of depth of penetration of austenitic steel are in the lower left portion of the plot, which indicates low values of welding current and low values of welding frequency. Higher values of penetration are in the upper and lower right portion of the plot, which indicates high values of welding current and at

both low and high welding frequency. As higher welding current is the cause of higher heat input, and it transfers huge amount of heat into the weld zone, large volume of molten weld pool and high depth of penetration may have been created. Variation of pulsing frequency is not found to show a clear trend on influencing depth of penetration, although, on the whole, lower pulsing frequency shows higher penetration.

The contour plot and surface plot of height of reinforcement (HOR) with the variation of welding voltage and welding pulse frequency, while torch travel speed is kept constant at 90 mm/min, 120 mm/min and 150 mm/min are shown in **Fig.8** and **Fig.9, Fig.10**, **Fig.11, Fig.12** and **Fig.13** respectively.

In case of constant torch travel speed of 90 mm/min and 120 mm/min, it can be observed that the highest values of height of reinforcement of austenitic steel are in the lower right portion of the plot, which indicates high values of welding current and low values of welding frequency. The lowest values of height of reinforcement for constant torch travel speed of 90mm/min and 120 mm/min are in the upper left side of the plot, which indicates low values of welding current and increasing values of welding frequency from middle to high values. In case of constant torch travel speed of 150 mm/min, lowest values of height of reinforcement of austenitic steel are in the lower left part of the plot, which indicates low values of welding current and welding frequency; higher values are in the upper right portion of the plot, which indicates high values of welding current and welding frequency. Higher heat energy input to the weld zone due to high welding current, may have caused higher volume of melted electrode and enlarged volume of weld zone. So, larger reinforcement height, with higher welding current, can be expected in bead-on-plate welding. Variation of pulsing frequency is not found to show a clear trend on influencing reinforcement.

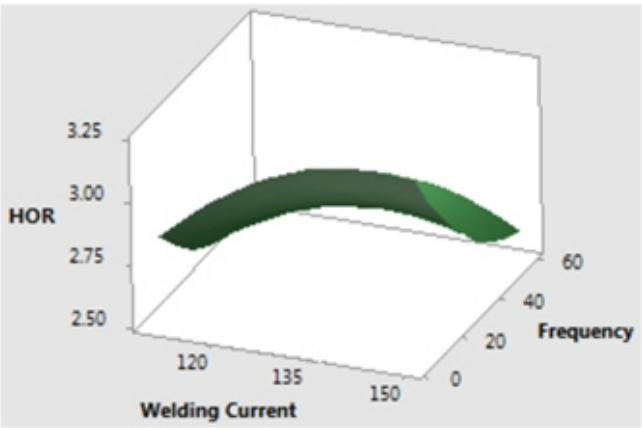


Fig. 9 : Surface plot of height of reinforcement with welding current and welding frequency at a stable torch travel speed of 90 mm/min

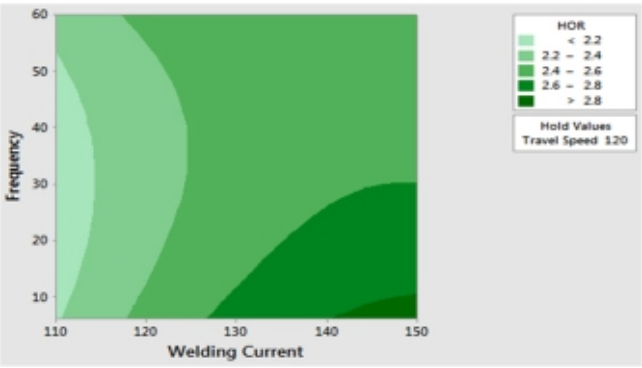


Fig.10 : Contour plot of height of reinforcement with welding current and welding frequency at a stable torch travel speed of 120 mm/min

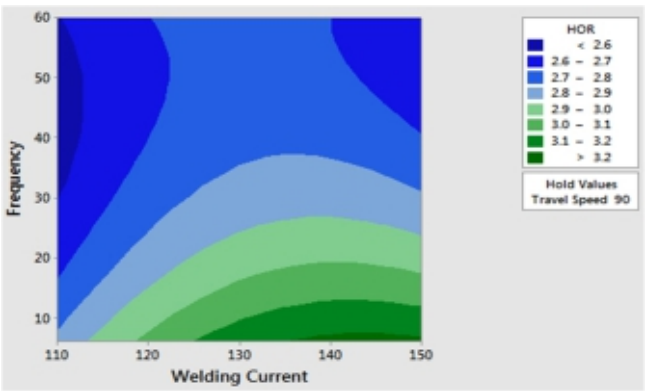


Fig. 8 : Contour plot of height of reinforcement with welding current and welding frequency at a stable torch travel speed of 90 mm/min

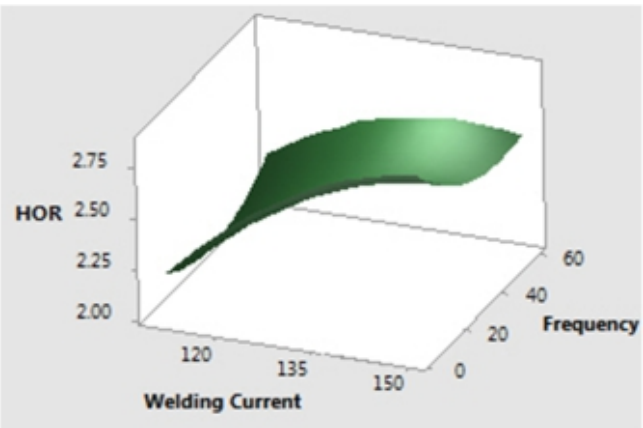


Fig.11 : Surface plot of height of reinforcement with welding current and welding frequency at a stable torch travel speed of 120 mm/min

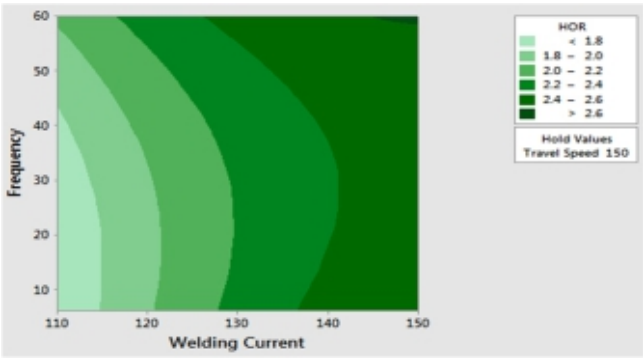


Fig.12 : Contour plot of height of reinforcement with welding current and welding frequency at a stable torch travel speed of 150 mm/min

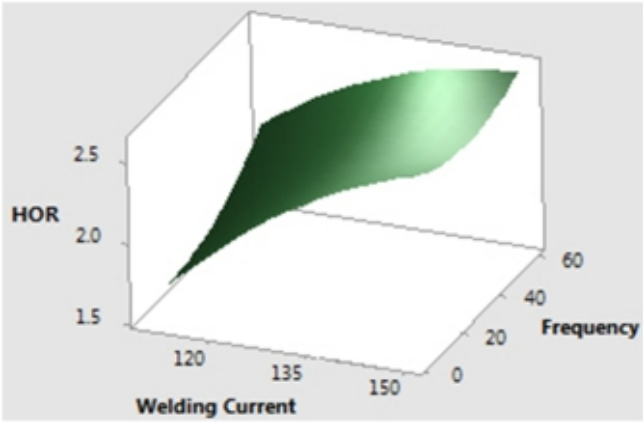


Fig.13 : Surface plot of height of reinforcement with welding current and welding frequency at a stable torch travel speed of 150 mm/min

in the upper right portion of the plot, which indicates high value of welding current and welding frequency.

As higher welding current is related to higher heat input to the system of welding creating higher volume of molten weld pool, some portion of molten electrode material is extended on the base plate, thereby increasing the bead width as also height of reinforcement. It also increases penetration to some extent. Therefore, uniformly, wider weld bead is formed with higher welding current. However, no clear tendency of bead geometry parameters on the variation of welding pulse frequency can be revealed from the experimental observations made in this work, although, on the whole, lower pulsing frequency intends to give higher bead width when weld current is high.

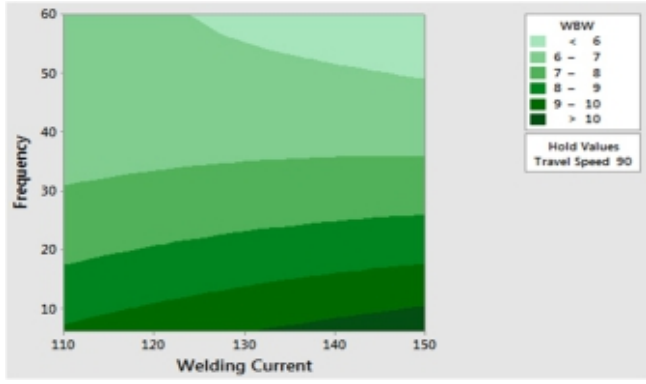


Fig. 14 : Contour plot of weld bead width with welding current and welding frequency at a stable torch travel speed of 90 mm/min

The contour plot and surface plot of weld bead width (WBW) with the variation of welding voltage and welding frequency, while torch travel speed being kept constant at the lower value of 90 mm/min, middle value of 120 mm/min and higher value of 150 mm/min are shown in **Fig.14** and **Fig.15, Fig.16** and **Fig.17**, **Fig.18** and **Fig.19** respectively. In case of constant travel speed of 90mm/min, 120 mm/min and 150 mm/min, it can be observed that the highest values of weld bead width of austenitic steel are in the lower right portion of the plot, which indicates high value of welding current and low value of welding frequency. The lowest values of weld bead width for a constant torch travel speed of 120 mm/min and 150 mm/min are in the left side of the plot, which corresponds to low values of welding current and increasing values of welding frequency from middle to high values. But in case of constant torch travel speed of 90 mm/min, the lowest values of weld bead width are

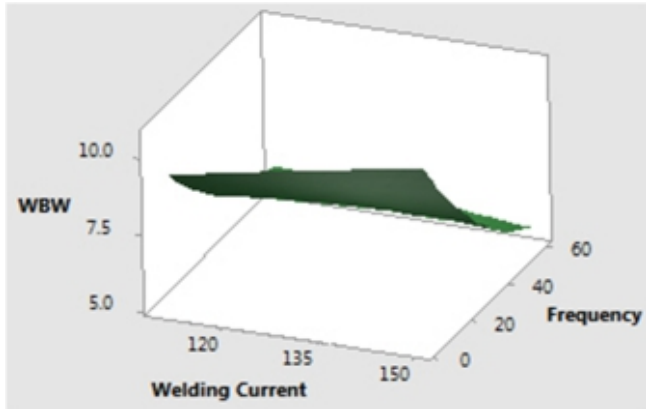


Fig.15 : Surface plot of weld bead width with welding current and welding frequency at a stable torch travel speed of 90 mm/min

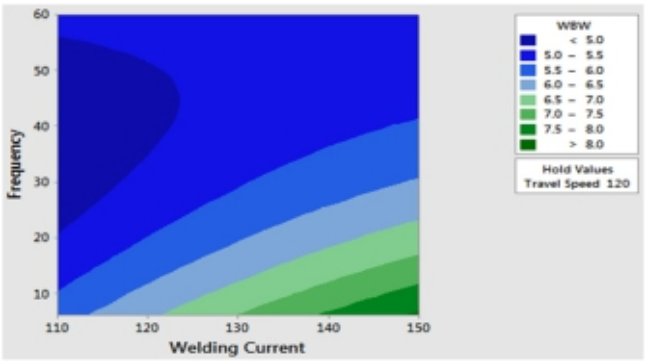


Fig.16 : Contour plot of weld bead width with welding current and welding frequency at a stable torch travel speed of 120 mm/min

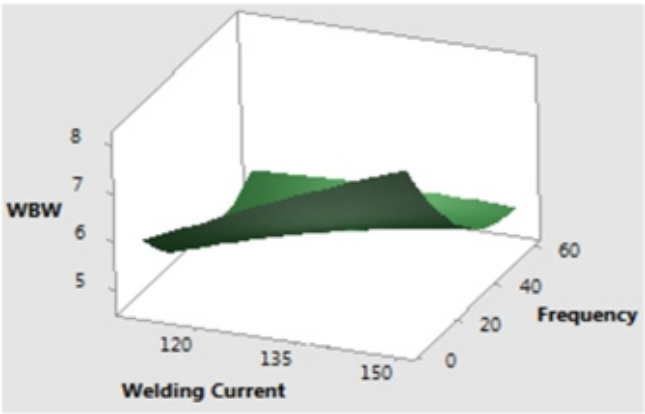


Fig.17 : Surface plot of weld bead width with welding current and welding frequency at a stable torch travel speed of 120 mm/min

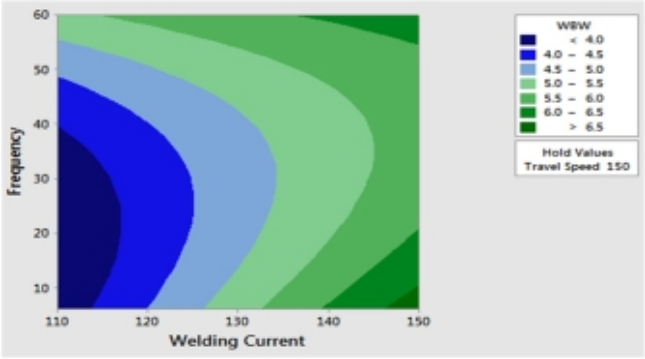


Fig.18 : Contour plot of weld bead width with welding current and welding frequency at a stable torch travel speed of 150 mm/min

With the increase in weld torch travel speed from 90 mm/min to 150 mm/min, lowering of weld bead width occurs naturally as increase in torch travel speed results in lowering of heat input as per equation (1) thereby causing lesser volume of molten material during welding. This not only reduces bead width, but also the height of reinforcement and also the

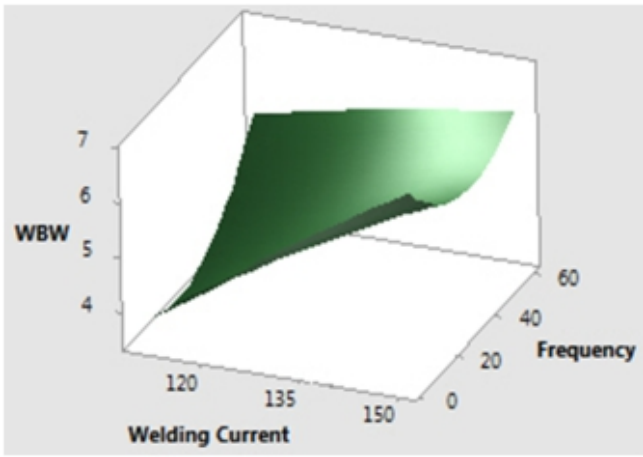


Fig.19 : Surface plot of weld bead width with welding current and welding frequency at a stable torch travel speed of 150 mm/min

penetration. This tendency can be revealed if one closely follows the range of values of the respective weld bead geometry parameters as shown in the contour plots of depth of penetration (DOP) in **Fig.2, Fig.4** and **Fig.6** height of reinforcement (HOR) in **Fig.8, Fig.10** and **Fig.12** and weld bead width (WBW) in **Fig.14, Fig.16** and **Fig.18.** Similar observations were also reported in some previous works [13,17,18].

In this experiment, clear trend of pulsing frequency influencing weld bead parameters cannot be noted. Pulsing is known to impart better penetration. In this experiment, higher pulsing frequency is found to lower penetration, and lower frequency gives higher penetration. However, in some cases, low as well as high pulsing frequency give high penetration. Similar type of lack of correlation exists in case of height of reinforcement and weld bead width. In fact, it was reported in an earlier work [1] that pulsing frequency was observed to influence dilution of stainless steel filler with the low carbon steel substrate thereby resulting in varying bond strength. Direct effect of pulsing on bead geometry was not observed in that work.

### 3.1.3 Recommended Parametric Combination for Cladding

After analysis of all weld bead geometry parameters obtained from bead-on-plate experiment by GTAW-P with their respective contour and surface plots and effect of heat input on depth of penetration, height of reinforcement and weld bead width, it is observed that utmost reinforcement is obtained in the present experiment at a heat input of 1.003 kJ/mm and moderate reinforcement is obtained at a heat input of 0.60 kJ/mm. However, minimum depth of penetration is obtained with heat input of 0.498 kJ/mm to 0.594 kJ/mm and moderate depth of penetration is obtained with heat input of 0.60 kJ/mm to 0.63 kJ/mm. Weld bead width is maximum at a heat input of

0.732 kJ/mm to 1.003 kJ/mm and moderate at a heat input of 0.594 to 0.63 kJ/mm. With the increase in heat input, heat supplied to the weld zone is increased causing higher volume of molten material. This large volume of molten material with high heat input results in high penetration and width and often some amount of reinforcement. However, for cladding, considerable low penetration with large width and reinforcement are the requirement, and hence, parametric conditions would be chosen considering this need of cladding.

As in cladding operation, low depth of penetration with higher reinforcement height and higher weld bead width is preferable, it may be suggested that the condition for imparting heat input of 0.594 kJ/mm, 0.60 kJ/mm and 0.63 kJ/mm can be applied in GTAW-P weld cladding practice. In the present case, (150A welding current, 33Hz welding frequency and 150 mm/min torch travel speed), (130A welding current, 33Hz welding frequency and 120 mm/min torch travel speed) and (150A welding current, 60Hz welding frequency and 120mm/min torch travel speed) are chosen to achieve the required heat input respectively.

### 3.2 Cladding Experiment to Evaluate the Lowest Corrosion Condition

Cladding is performed with austenitic stainless steel filler wire on the same 25 mm thick low carbon steel base plate as that of bead-on-plate experiment with pre-selected process parameters like welding current, welding frequency and torch travel speed as detailed in **Table 6**. These process variables are selected following the results obtained from bead-on-plate experiments done in the first phase of the present work using gas tungsten arc welding process under 100% argon gas shield with a gas discharge of 15 litre/min to obtain desired cladding situation. Similar gas shield and gas flow rate and commercially pure tungsten electrode with a diameter of 2.4 mm and wire type filler material of 1.2 mm diameter are also set for carrying out weld cladding experiments in GTAW-P to find out favourable process parameters towards achieving high resistance to corrosion under chloride environment.

Corrosion test is done the clad surface under a chloride environment. The corrosive medium is created by a mixture of 30 gm Ferric Chloride, 27 ml HCl and 73 ml distilled water to undertake accelerated corrosion test. Weight loss after immersion in a corrosive medium for 24 hours is noted. Rate of weight loss per unit area is considered to be one measure in the corrosion test. The other measure of corrosion has been the average number of pits per unit surface area of the clad part. Results of corrosion test of low carbon steel base plate and corrosion test of austenitic stainless steel clad test samples are shown in **Table 7** and **Table 8** respectively. **Table 8** shows the corrosion rate and number of pits/cm$^2$ of austenitic stainless steel clad test specimen at different heat input and other welding parameters. With the accelerated corrosion test, corrosion rate of as high as 417.917 gm/m$^2$.hr is noted for the base plate without any cladding, while a low corrosion rate of 118.75 gm/m$^2$.hr is found against a heat input of 0.59 kJ/mm for the clad specimen based on the two replicated experiments (sample A and sample B). Corrosion rate of austenitic stainless steel clad test specimen expectedly shows large reduction compared to that of the low carbon steel base plate. Austenitic stainless steel contains large amount of chromium, molybdenum, nickel, etc., which is considered to be the main cause behind its corrosion resistive property. Both corrosion rate and pit count/square cm area are found to increase with the increase of heat input within the range of the present experimental conditions.

After the corrosion test, corroded areas of test specimens are observed under advanced stereo microscope to count the number of pits occurred due to corrosion. Images of typical corroded samples with clear view of pits are shown in **Fig.20** through **Fig.22** and the counted numbers of pits are tabulated in **Table 8**.

Pitting is the result of localized corrosion to the exposed surface as small cavities, evenly distributed on the corroded surface with a rate of penetration that increases with time. From **Fig. 20** through **Fig. 22**, number of counted pits clearly indicates that number of pits per unit area (pitting frequency) is affected by heat input. Results show that number of pits increases with the increase of heat input, and it becomes quite

Table 6 : Heat input and other process parameters for cladding experiment

| Sl. No. | Sample No. | Welding Current (A) | Welding Frequency (Hz) | Torch Travel Speed (mm/min) | Heat Input (kJ/mm) |
|---|---|---|---|---|---|
| 1 | $TC_1$ | 150 | 33 | 150 | 0.59 |
| 2 | $TC_2$ | 130 | 33 | 120 | 0.6 |
| 3 | $TC_3$ | 150 | 60 | 120 | 0.63 |

large at a heat input of 0.63 kJ/mm with a number of 1189 per one square cm area. At higher heat input, austenite may be transformed into sigma phase causing more corrosion characteristic as was observed in some previous investigations. Therefore, lower heat input of 0.59 kJ/mm may be adopted for GTAW-P cladding to have low corrosion and thereby, guaranteeing higher service life of clad components.

Table 7 : Results of corrosion test of low carbon steel base plate

| Sl. No. | Base Plate | Weight loss (gm) | Corrosion Rate ($gm/m^2.hr$) |
|---|---|---|---|
| 1 | Low carbon steel | 1.003 | 417.917 |

Table 8 : Results of corrosion test of austenitic stainless steel clad test samples by GTAW-P process

| Sample | | Welding Current (A) | Welding Frequency (Hz) | Torch Travel Speed (mm/min) | Heat Input (kJ/mm) | Weight Loss (gm) | Corrosion Rate ($gm/m^2.hr$) | Average Corrosion Rate ($gm/m^2.hr$) | Number of Pits ($count/cm^2$) |
|---|---|---|---|---|---|---|---|---|---|
| $TC_1$ | A | 30 | 175 | 420 | 0.59 | 0.279 | 116.16 | 118.75 | 663 |
| | B | | | | | 0.291 | 121.34 | | |
| $TC_2$ | A | 25.5 | 210 | 360 | 0.6 | 0.383 | 159.7 | 162.29 | 775 |
| | B | | | | | 0.396 | 164.88 | | |
| $TC_3$ | A | 30 | 210 | 390 | 0.63 | 0.497 | 207 | 209.59 | 1189 |
| | B | | | | | 0.509 | 212.18 | | |

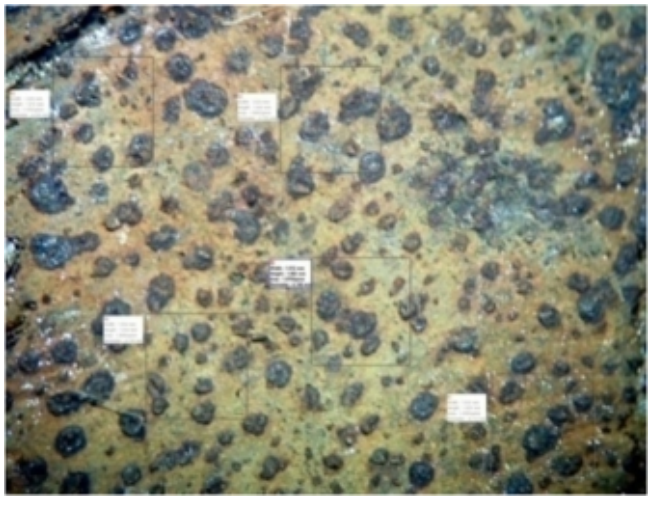

Fig.20 : Typical area of corroded test sample (TC1)
[Area of this clad portion is (6.54×4.84) $mm^2$,
No. of pits counted = 663/$cm^2$, Heat Input = 0.594 kJ/mm]

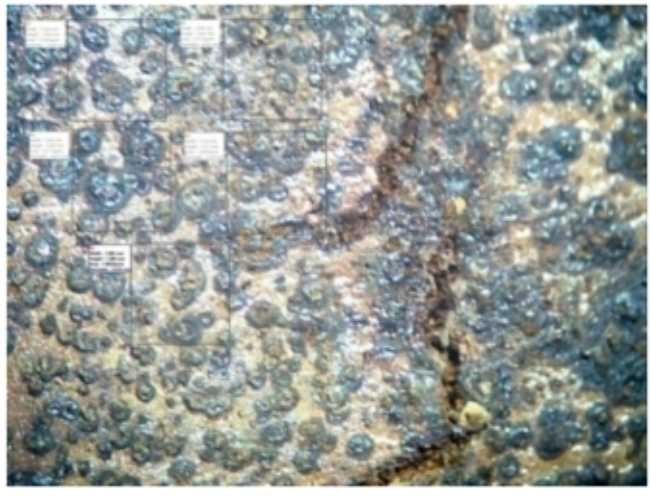

Fig.21 : Typical area of corroded test sample (TC2)
[Area of this clad portion is (6.54×4.84) $mm^2$,
No. of Pits counted = 775/$cm^2$, Heat Input = 0.6 kJ/mm]

## 4.0 Conclusion

Results obtained from this experiment on weld bead formation and cladding performance on low carbon steel base substrate by 316 austenitic stainless steel filler wire using Pulsed GTAW process lead to the following conclusions:

- Depth of penetration, height of reinforcement and weld bead width increase with increasing heat input, that is, by increasing welding current and decreasing torch travel speed, with little deviation for GTAW-P bead-on-plate experiment.

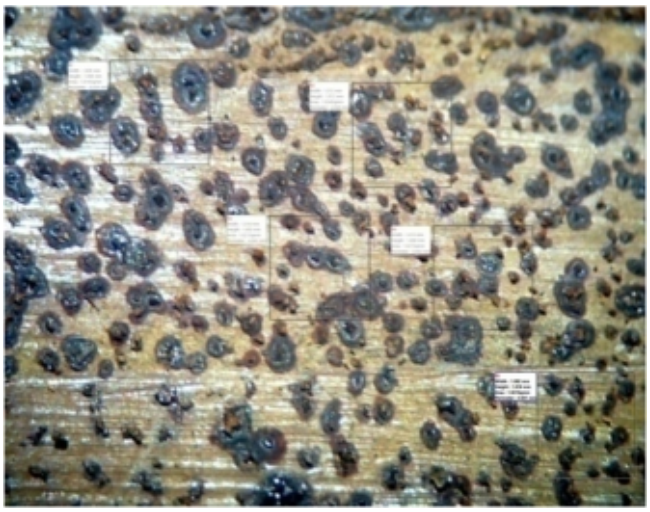

Fig. 22 : Typical area of corroded test sample ($TC_3$)
[Area of this clad portion is (6.54×4.84) $mm^2$
No. of Pits count = 1189/$cm^2$, Heat Input =0.63 kJ/mm]

- On the basis of all observations made in bead-on-plate experiments, it may be suggested that the condition for imparting heat input of 0.594kJ/mm, 0.60kJ/mm and 0.63kJ/mm can be adopted in GTAW-P weld cladding practice as it gives low penetration along with good amount of reinforcement and bead width.
- Results of corrosion test clearly point out that increasing heat input increases corrosion rate and number of pits per unit area of cladding with 316 austenitic stainless steel filler wire in GTAW-P cladding processes. At higher heat input, solidification time is more and there may be possible transformation of austenite to sigma phase. This may have increased corrosion rate.
- In the present experimental investigation on cladding using GTAW-P, the least corrosion rate is found at the lowest heat input of 0.594 kJ/mm with 150A welding current, 33Hz pulsing frequency and 420 mm/min torch travel speed, and this condition can be recommended to the industry to adopt.

## Acknowledgement

The present paper is a revised version of an article presented in the 5th International Congress (IC 2020) of the International Institute of Welding held in Mumbai on February 6-8, 2020 and organized by the Indian Institute of Welding.

## References

[1] Ishida T (1991); Formation of stainless steel layer on mild steel by welding arc cladding, Journal of Materials Science, 26, pp. 6431–6435.

[2] Cheng FT, Lo KH Lo, Man HC (2003); NiTi cladding on stainless steel by TIG surfacing process Part I. Cavitation erosion behavior, Surface and Coatings Technology, 172, pp. 308–315.

[3] Xu G, Kutsuna M, Liu Z, Yamada K (2006); Comparison between diode laser and TIG cladding of Co-based alloys on the SUS403 stainless steel, Surface and Coatings Technology, 201(3-4), pp. 1138-1144.

[4] Wang XH, Zhang M, Zou ZD, Song SL, Han F, Qu SY (2006); In situ production of Fe–TiC surface composite coatings by tungsten-inert gas heat source, Surface & Coatings Technology, 200(6), pp. 117–6122.

[5] Lv SX, Xu ZW, Wang HT, Yang SQ (2008); Investigation on TIG cladding of copper alloy on steel plate, Science and Technology of Welding and Joining, 13(1), pp. 10–16.

[6] Chen JH, Hua PH, Chen PN, Chang CM, Chen MC, Wu W (2008); Characteristics of multi-element alloy cladding produced by TIG process, Materials letters, 62(16), pp. 2490-2492.

[7] Madadi F, Ashrafizadeh F, Shamanian M (2012); Optimization of pulsed TIG cladding process of stellite alloy on carbon steel using RSM, Journal of Alloys and Compounds, 510(1), pp. 71-77.

[8] Azimi GH, Shamanian M, Firozi P (2012); Microstructure and wear properties of Fe-Cr-C and Fe-Cr-Nb-C clads on carbon steel by TIG surfacing process, International Journal of Surface Science and Engineering, 6(1-2), pp. 15-23.

[9] Saha MK, Das S (2016); A review on different cladding techniques employed to resist corrosion, Journal of the Association of Engineers, India, 86, pp. 51–63.

[10] Westin EM, Schnitzer R, Ciccomascolo F, Maderthoner A, Gronlund K, Runnsjo G (2016); Austenitic stainless steel bismuth-free flux-cored wires for high-temperature applications, Welding in the World, 60(6), pp. 1147-1158.

[11] Khara B, Mandal N D, Sarkar A, Sarkar M (2016); Weld Cladding with Austenitic Stainless Steel for Imparting Corrosion Resistanc, Indian Welding Journal, 49(1), pp. 74-81.

[12] Sahoo CK, Masanta M (2017); Microstructure and mechanical properties of TiC-Ni coating on AISI304 steel produced by TIG cladding process, Journal of Materials Processing Technology, 240, pp. 126-137.

[13] Saroj S, Sahoo CK, Masanta M (2017); Microstructure and mechanical performance of TiC-Inconel825 composite coating deposited on AISI 304 steel by TIG

cladding process, Journal of Materials Processing Technology, 249, pp. 490-501.

[14] Verma AK, Biswas BC, Roy P, De S, Das S (2017); An investigation on the anti-corrosion characteristic of stainless steel cladding, Indian Welding Journal, 50(3), pp. 52–63.

[15] Roy S, Samaddar S, Uddin N Md, Hoque A, Mishra S, Das S (2017); Effect of Activating Flux on Penetration in ATIG Welding of 316 Stainless Steel, Indian Welding Journal, 50(4), pp. 72 – 80.

[16] Olivares EAG, Díaz VMV (2018); Study of the hot-wire TIG process with AISI-316L filler material analysing the effect of magnetic arc blow on the dilution of the weld bead, Welding international, 32(2), pp. 139-148.

[17] Saha S, Das S (2018); Investigation on the Effect of Activating Flux on Tungsten Inert Gas Welding of Austenitic Stainless Steel Using AC Polarity, Indian Welding Journal, 51(2), pp. 84 – 92.

[18] Saha MK, Hazra R, Mondal A, Das S (2018); On corrosion resistance of austenitic stainless steel clad layer on a low alloy steel, Indian Science Cruiser, 32(3), pp. 66–72.

[19] Zhang Z, Mee VVD, Golding M, Donate J, Malioglou A (2019); Pitting corrosion resistance properties of super duplex stainless steel weld metals and influencing factor, Welding in the World, 63(3), pp. 617-625.

[20] Saha MK, Hazra R, Mondal A, Das S (2019); Effect of heat input on austenitic stainless steel weld bead on low carbon steel, Journal of The Institution of Engineers (India): Series C, 100(4), pp. 607-615.